

Full Length Article

Combustion of *n*-butyl acetate synthesized by a new and sustainable biological process and comparisons with an ultrapure commercial *n*-butyl acetate produced by conventional Fischer esterification

Yujie Wang^a, Zhu Chen^b, Matthew Haefner^a, Songtao Guo^a, Nicholas DiReda^a, Yuechao Ma^b, Yi Wang^b, C. Thomas Avedisian^{a,*}

^a Sibley School of Mechanical and Aerospace Engineering, Cornell University, Ithaca, NY 14853, United States

^b Department of Biosystems Engineering, Auburn University, Auburn, AL 36849, United States



ARTICLE INFO

Keywords:

Butyl acetate
Droplet combustion
Biofuels
Soot
Microgravity
genome engineering

ABSTRACT

This paper reports a study of the combustion dynamics of *n*-butyl acetate (BA) using the configuration of a burning droplet. Two grades of BA were examined: one (SBA) synthesized by a new process described in the paper that uses a metabolically engineered solventogenic *Clostridium* strain through an extractive fermentation process using *n*-hexadecane as the extractant; and one commercially available as a high-purity (99.9%) 'neat' BA grade produced by conventional Fischer esterification (NBA). The initial droplet diameter was primarily 0.6 mm with some limited experiments carried out for 0.4 mm droplets to show the influence of convection. Experiments were performed in the standard atmosphere and ignition was by spark discharge. The results showed the presence of impurities in the SBA at mass concentrations totaling about 6% which included *n*-butanol, *n*-hexadecane, iso-propyl alcohol and ethyl acetate. Droplet burning rates and flame structures were not influenced by these impurities at this concentration level. In the presence of convection created by buoyancy, droplets burned faster with stretched flames and a luminosity revealing the presence of soot by incandescence at the flame tips. Reducing the initial droplet diameter to 0.4 mm eliminated the convective effect and resulted in near spherical flames. The results presented show that the new synthesis process is a sustainable alternative for BA production with burning characteristics identical to NBA in both convective and stagnant gas transport fields.

1. Introduction

The promise of biofuels lies in their potential to provide a sustainable alternative to fossil fuels that power energy systems such as combustion engines especially when blended with such fuels. Their development comes at a time of renewed interest in reducing greenhouse gases and particulate emissions from ground transportation vehicles. For example, fuel economy standards are being proposed in the United States that will require automobiles to reach 51 miles per gallon by 2026 [1]. Blending biofuels with petroleum fuels (e.g., diesel, gasoline) is an effective way to realize a volumetric reduction of fossil fuels with generally favorable impacts on particulate and gaseous emissions. At the same time, blending biofuels with neat petroleum fuels typically results in heats of combustion that are lower than the petroleum fuel [2], and blending can reduce fuel economy.

Many biofuels have recently been considered as additives to

petroleum fuels to replace the widely used ethanol. Detailed screening processes have been developed to aid in the selection. For example, a tiered process of screening was developed based on fuel properties such as boiling point, freezing point, miscibility with hydrocarbons, vapor pressure and oxidation stability among others [3,4]. A 'merit' function (MF) for gasoline blending was described [5] based on a formula which included a number of thermal properties to screen various biofuels: the higher the MF, the more attractive would be the biofuel as a blendstock for gasoline.

Among the biofuels considered for blending with gasoline or diesel are esters. Their production can be renewable and environmentally friendly [6,7]. *n*-butyl acetate (BA; C₆H₁₂O₂, BP = 399 K, MP = 195 K, ρ_L = 885 kg/m³) in particular has favorable properties as a sustainable biofuel additive to petroleum fuels, including considerations of freezing, boiling and flash points [2]. As an oxygenated compound, BA shares with other biofuels a propensity to reduce (though not completely eliminate) particulate emissions through mechanisms based on carbon/

* Corresponding author.

E-mail address: cta2@cornell.edu (C. Thomas Avedisian).

<https://doi.org/10.1016/j.fuel.2021.121324>

Received 10 April 2021; Received in revised form 15 June 2021; Accepted 20 June 2021

Available online 10 August 2021

0016-2361/© 2021 Elsevier Ltd. All rights reserved.

Nomenclature

a	ellipse major axis
b	ellipse minor axis
D	droplet diameter
D_f	flame diameter
D_o	initial droplet diameter
K_o	burning rate for $g = 0$
K_c	burning rate for $g \neq 0$
g	gravitational constant (m/s^2)
Gr	Grashof number
t	time (s)
T_f	flame temperature (K)
T_d	droplet temperature (K)
v_B	velocity induced by buoyancy
v_S	'Stefan' velocity induced by fuel evaporation
ℓ	characteristic length in definition of Grashof number
β	thermal expansion coefficient
$\rho \leftarrow L$	liquid density
ρ_g	average gas density
ν	average gas kinematic viscosity

oxygen bonds in the biofuel molecule which restrict carbon from becoming incorporated into soot [8]. Several concerns need to be addressed before BA can become a commercial additive to petroleum fuels. A sustainable method of production must be developed that can produce BA in the quantities needed to meet the needs of the transportation sector. In 2019, this need would have been almost five billion gallons for biofuel additives to diesel fuel at a 10% loading [9].

BA is conventionally produced by the Fischer esterification process. Fischer esterification usually needs a strong acid (such as sulfuric acid) as the catalyst, which could be turned into waste making the process environmentally unfriendly [6,10,11]. The production process consumes comparatively high energy as the reactions are carried out at 60–110 °C. In comparison, the microbial fermentation process we describe could be carried out at room temperature and be more selective for BA production.

The choice of BA as a fuel additive includes consideration of its boiling point of 399 K, solubility in the fuel, flash point, and factors such as its influence on the fuel vaporization rate, ignition characteristics, potential for flash boiling to occur through preferential vaporization and bubble nucleation processes, and others. Regarding fundamental assessments of performance, an adequate supply of BA produced by a new synthesis process is required given that bench-scale production processes will typically be expected to have a comparatively low yield in the first instance. The burning configuration to evaluate performance must accommodate limited supplies. The expectation of small production volumes (less than 1 L) precludes initial performance evaluation in large scale and end-use configurations such as combustion engines or industrial furnaces which will require tens of liters at a time.

During the synthesis of BA, miscible by-products may form which render the product a multicomponent mixture. The concentration and thermal properties of the components can influence the burning characteristics such that the synthesized BA ('SBA') burns differently than the ultrapure variant of BA or neat BA ('NBA') which is the benchmark for comparison. It is important to understand the effect of the by-products on the combustion physics of the mixture and how SBA ultimately compares with NBA. This paper addresses this matter. A new synthesis process is outlined in Section 2. Experiments are reported to examine the effect of the by-products on the burning process.

Two broad matters are addressed in the paper: a new process for producing NBA; and the combustion characteristics of NBA and SBA. The results reported fill a gap in the understanding of BA combustion

which appears to have been viewed only through the lens of catalytic combustion and decomposition [12–21].

2. Synthesis of butyl acetate

The conventional process for producing BA is by Fischer esterification. This process involves a reaction that converts carboxylic acids to esters and water in the presence of alcohols and an inorganic catalyst. Impurities are removed by distillation and a very high-purity BA can result. In the present study, a high-purity commercial product from this process by Sigma Aldrich (St. Louis, MO) with a stated purity of 99.9% (Sigma product number 442666-U) is the benchmark NBA for the comparisons reported in the present study.

The production of NBA by Fischer esterification consumes a comparatively high amount of energy and generates toxic wastes [6] as it usually needs a strong acid (e.g., sulfuric acid) as the catalyst which can be a waste product. The reactions need to be carried out at elevated temperatures, 60–110 °C. On the other hand, the microbial fermentation process described here can be carried out at room temperature with greater selectivity for BA production. The method of synthesizing BA is briefly described below with further details given in [22].

We hypothesized that solventogenic clostridia can be an excellent microbial platform for BA production by taking advantage of its natural pathways for co-producing acyl-CoAs (acetyl-CoA and butyryl-CoA), fatty acids (acetate and butyrate), and alcohols (ethanol and butanol) either as intermediates or end-products. Through systematic genome engineering we developed a specific strain, *C. saccharoperbutylacetonicum* FJ-1201, with potential yields of 20.3 g/L BA using monosugars (glucose and xylose) which could be generated from lignocellulosic biomass as the substrate in an extractive batch fermentation process with *n*-hexadecane as the extractant [22]. After fermentation, the SBA that results is a mixture of NBA and various by-products as listed in Table 1.

The BA produced in the process is NBA which, as noted in Table 1, is diluted by the four organics listed and water at the indicated mass concentrations which amount to 6%. At this level, the burning characteristics of NBA could be influenced by the dissolved by-products. This aspect is considered in Section 5.

It should be noted that the process as described above using the *Clostridium* strain was specific to BA production with high selectivity. However, it can be applied to other organics such as *n*-butanol, butyl butyrate, and longer chain hydrocarbon molecules through systematic metabolic engineering of the microbial pathways. The product yields would be dependent on the molecule of interest.

3. Burning configuration for SBA and NBA

The initial effort to synthesize SBA in a bench-scale experimental design has yielded several tens of milliliters at a time. Such a quantity is insufficient for testing in large scale combustion configurations such as engines. An alternative platform to accommodate small production volumes was instead selected for studying SBA combustion: an isolated droplet burning under conditions that promote spherical droplet flames with a 1-D gas transport originating by minimizing the presence of forced and natural convection. Fig. 1a is a schematic. There are several reasons for this choice.

The cost of NBA at over \$2100 USD/L can make combustion engine testing economically impractical. For the initial droplet diameter of the present study, 0.6 mm, volumes on the order of only 10 μ L per experiment are needed. The data reported here were obtained with an SBA and NBA fuel supply of less than 500 ml.

Simulations needed for validating combustion kinetic mechanisms are usually obtained using detailed numerical models from commercial codes. The experimental conditions typically eliminate the liquid phase by prevaporizing it so that complications associated with droplet/gas couplings which influence the chemistry of ignition [24] are not

Table 1
SBA and by-products (property data from [23]).

chemical →	NBA	<i>n</i> -butanol	<i>n</i> -hexadecane	<i>iso</i> -propanol	ethyl acetate	water vapor	unknown
formula →	C ₆ H ₁₂ O ₂	C ₄ H ₁₀ O	C ₁₆ H ₃₄	C ₃ H ₈ O	C ₄ H ₈ O ₂	H ₂ O	–
mass fraction (%)	94.3	3.8	0.4	0.134	0.118	0.865	0.383
boiling point (K)	399	391	560	356	350	373	–
critical point (K)	579	563	722	508	523	647	–

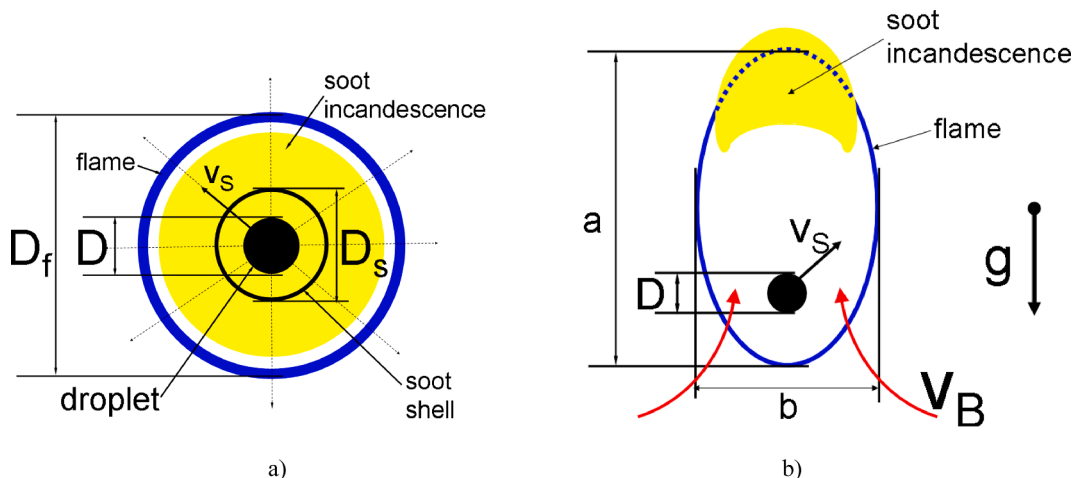


Fig. 1. a) Schematic of idealized 1-D droplet burning configuration. b) Schematic of 2D axisymmetric flame in the presence of buoyancy under gravity 'g'.

considered. With droplets present, the computational challenges are considerable but the results will be useful for validating the more complex configuration of 1-D droplet burning where fuel evaporation, unsteady gas and liquid transport, multicomponent mixture, radiation and sooting effects can be considered [25–29]. Simulations are not included in the present study because reduced kinetic mechanisms for BA are currently not available. The data developed as part of the present study should be useful for validating BA's kinetic mechanism for the 1-D droplet burning case. The data in the figures presented here are included in the Supplementary Material section.

4. Experiment

A brief description of the experimental design to create the configurations in Fig. 1 is provided in this section. Further details are given in [25,29,30]. The experiments were carried out under carefully controlled conditions to promote a one-dimensional gas transport. For 1-D gas transport there should be no relative velocity between the droplet and surrounding ambience. Such conditions were created by restricting the movement of test droplets in a stagnant gas (the standard atmosphere in the present study) and minimizing the effects of buoyancy by carrying out the experiments with a sealed free-fall chamber. Droplets were deployed onto two intersecting 14 μm diameter SiC fibers to prevent them from moving within a sealed chamber filled with room temperature air at atmospheric pressure. The chamber was mounted onto a metal frame with two cameras attached. The entire package is released into free fall during which the droplets are ignited and their burning histories recorded. The experimental time is about 1.2 s and the initial droplet diameters for most of the experiments reported here was 0.6 mm.

Ignition was achieved by electrical discharges from two sparks positioned on opposite sides of the droplet, though we found little difference in the burning process when one spark or two sparks were employed. Ignition was initiated 200 ms into free-fall. The spark duration was approximately 600 μs. The electrodes supporting the sparks were spring-loaded in solenoids to enable rapid retraction and precise re-positioning of the electrode tips after each experiment. Fig. 2 shows

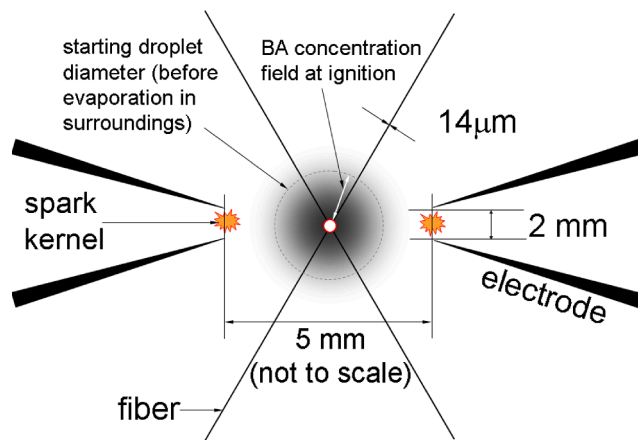


Fig. 2. Top view schematic of process for setting initial droplet diameter. Gray shading depicts the BA concentration gradient created by evaporation of the droplet from the initial size (gray dotted circle) to the desired size (red circle). Electrodes are rapidly retracted after ignition. Not to scale. (For interpretation of the references to color in this figure legend, the reader is referred to the web version of this article.)

the arrangement of a droplet relative to the electrodes with approximate dimensions indicated.

Droplet burning was recorded using two cameras in perpendicular directions. One view provided backlit images from a high-speed black and white (BW) camera at 200 frames/s and 4MP per image and the other provided color views of self-illuminated flames using a color camera at 30 frames/s. The light source for the BW camera was provided by a single wavelength LED (Prismatix Mic-LED with BLCC-04; 637 nm).

Using the video recordings of the burning process, droplet diameter measurements (D) were made using an analysis program that extracted these measurements in an automated way over the collection of images for a given burning event [31]. A circle fit to the droplet shape was

assumed because the BW images in the videos did not show any discernable deviation of cross-sectional shape from circular. The droplet boundary could be determined to within 3 pixels. With a calibration factor of 0.002 mm/pixel, the uncertainty of droplet diameter was approximately ± 0.006 mm.

Measurements of flame diameters (D_f) could not be automated because the flame boundaries were not sharp (a characteristic of droplet flames). Moreover, the flame boundary was less sharp than the droplet boundary with a higher pixel calibration factor: 0.014 mm/pixel for the color camera used. D_f therefore had to be obtained by a manual process. We used the ImagePro Plus (Rockville, MD, USA) software program coupled with a 24 in. Dell 4 K HD monitor to manually overlay flame images with a virtual ellipse because flame shapes were not entirely circular as shown in Fig. 5. Measurements were made of major ('a') and minor ('b') axes to obtain an equivalent diameter of $(a \times b)^{1/2}$. Operator skill was required to position the ellipse for each image. Different operators were calibrated against each other for consistency. The flame boundary could be determined to within approximately 8 pixels giving an uncertainty in D_f of approximately ± 0.112 mm.

The initial droplet diameter (D_0) was fixed at 0.6 mm so that D_0 would not be an added variable in the experiments [30]. This size was large enough to provide good image clarity for most of the burning history yet small enough that a large fraction of the burning history could be recorded. Some limited experiments were also carried out for $D_0 = 0.4$ mm to show the effect of droplet size on buoyancy and flame shape. The smallest diameter measured with the optical arrangement was approximately 0.1 mm. For each condition three or four repetitions were carried out.

Precise control of the initial droplet diameter was achieved using the process schematically illustrated in Fig. 2. Before the period of free-fall, a droplet of approximately 0.8 mm (dotted gray circle in Fig. 2) was first deployed onto the fibers by using a piezoelectric generator to propel droplets onto the intersection of the fibers. The droplet was then allowed to evaporate in the surrounding still air until the desired D_0 was reached, here being 0.6 mm. During evaporation an image of the droplet was projected on a monitor until it filled a virtual circle displayed on the monitor of the desired D_0 . A fairly precise and repeatable initial droplet diameter could be formed in this way with a precision of ± 0.005 mm for droplets.

The method in Fig. 2 of setting D_0 is most applicable to single component fuels. If the fuel is multicomponent, the waiting time for the droplet to evaporate down to the size of interest can induce changes of the droplet composition prior to ignition due to preferential evaporation while vaporizing in air. This problem was noted previously [29]. As a result, the initial concentration would not necessarily be the one prepared. It depends on the evaporation rate and internal diffusional resistance of species transport to the droplet surface.

With the above method of setting D_0 the gases surrounding the droplet will initially comprise a fuel-rich mixture of BA. The effect of this pre-existing vaporized BA on burning was assessed by comparing burning of NBA droplets formed as noted above with droplets immediately ignited after deployment with little to no pre-vaporization. The evolutions of scaled droplet and flame diameters ignited either immediately after deployment or after first vaporizing down to the desired size (0.6 mm) are shown in Figs. 3 and 4, respectively¹. The data show that the burning process for the two cases are nearly identical. This shows that the vaporized BA in Fig. 2 is either diffused away from the droplet or burned off quickly after ignition, and either possibility does not influence burning.

Limited experiments were also carried out for SBA and NBA droplets burning in a buoyant atmosphere to assess the efficacy of SBA to replicate NBA under convective burning conditions. Fig. 1b is a schematic of

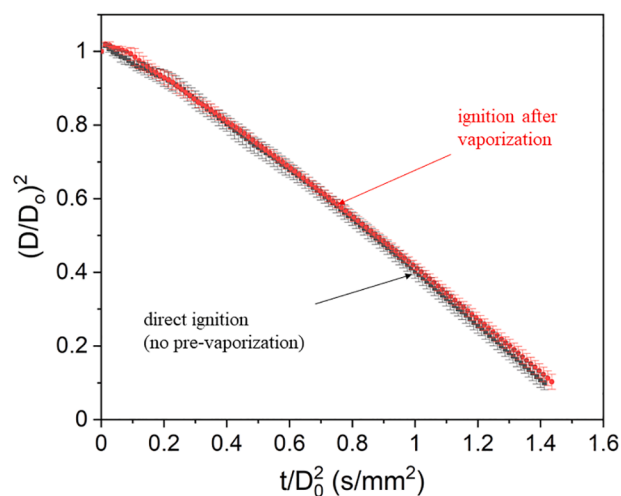


Fig. 3. Evolution of average scaled droplet diameters for $D_0 = 0.6$ mm for NBA droplets ignited after 0.8 mm droplets were evaporated down to 0.6 mm then ignited, and NBA droplets deployed at approximately 0.6 mm and ignited immediately after deployment with no pre-vaporization.

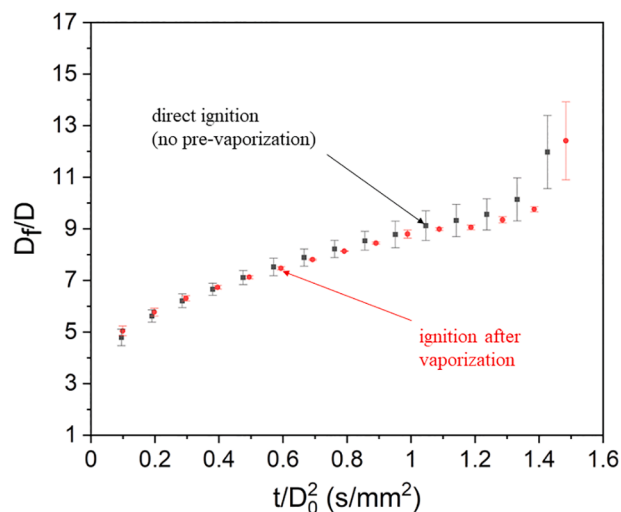


Fig. 4. Evolution of average scaled flame diameters for $D_0 = 0.6$ mm for NBA droplets ignited after 0.8 mm droplets were evaporated down to 0.6 mm then ignited, and NBA droplets deployed at approximately 0.6 mm and ignited immediately after deployment with no pre-vaporization.

the convective flame configuration. In practice, BA droplets will be evaporated in the presence of a strong convective field. A simple way to assess the influence of convective burning is to observe the burning process in a flow created entirely by buoyancy in earth's normal gravity. This was accomplished by deploying, and then igniting, a test droplet in the sealed chamber and allowing the droplet to burn but without releasing the package into free-fall. Though less controllable than imposing a forced air flow around a droplet, the buoyant flow exerts a similar influence on evaporation. The results are discussed in Section 5.

SBA is more complex than NBA because SBA is a multicomponent mixture. The effect of gas motion around SBA droplets could influence the droplet temperature, internal flow dynamics, and distribution of dissolve species inside SBA droplets by the concentration gradients that are developed by internal liquid motion induced by shear-induced mixing inside SBA droplets. These matters are discussed further in Section 5.2.

¹ Data plotted in all of the figures in the paper are provided in the Supplementary Materials section of the journal.

5. Results and discussion

5.1. Droplet flame structures

Selected photographs of droplet flames for NBA, SBA, and by-products formed during synthesis of BA (Table 1) are shown in Fig. 5 for burning without external convection. The time scale at the bottom is in seconds after ignition and $D_0 = 0.6$ mm.

The luminosity of the NBA and SBA flames in Fig. 5 reveals the presence of soot aggregates even though NBA is an oxygenate. Flame luminosity is indicative of soot incandescence and the amount of soot formed [32], and the bright yellow flame color is due to the wavelength

of the light emitted in the visible light spectrum[33]. Of the SBA by-products in Table 1, only hexadecane has a sooting propensity high enough to where soot shells are visible. However, no soot shells are seen for SBA so SBA flame luminosity is not attributed entirely to dissolved hexadecane as a source of soot. A speculation is that as the fuel evaporates and the gases flow radially outward toward the flame the oxygenate delays the formation of soot to temperatures higher than the conventional soot inception temperature. With soot particle ignition closer to the high temperature regions of the flame, ignited soot aggregates could burn up more quickly before a soot shell fully forms.

The flame shapes for the SBA by-products were generally spherical throughout burning because of the expected minimal effect of buoyancy

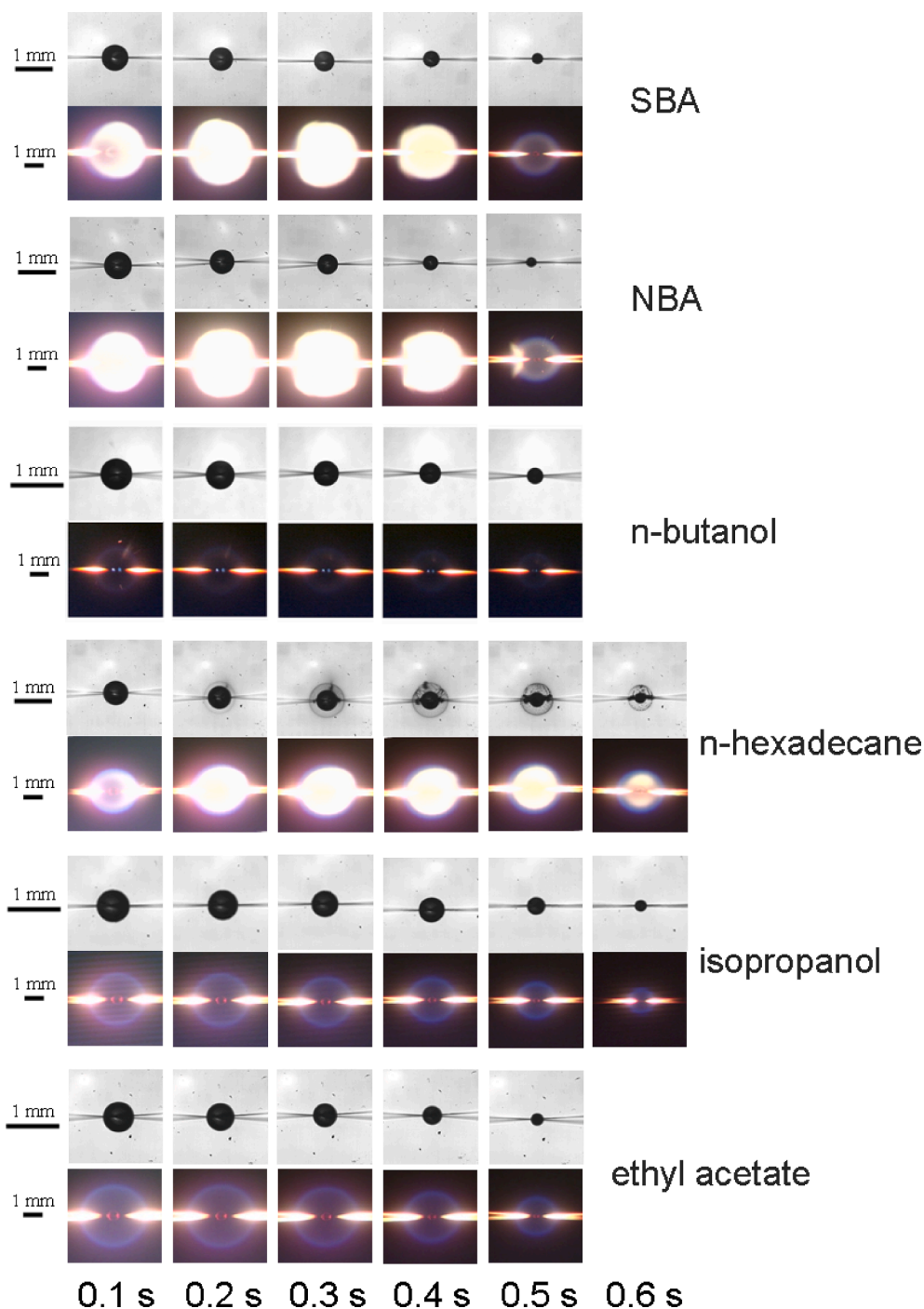


Fig. 5. Selected images of NBA and SBA combustion without convection, including dissolved by-products. Time after ignition is shown. *n*-butanol photographs are from [41]. For SBA and NBA the flames are non-sooting at 0.5 s. A soot shell is visible for *n*-hexadecane. $D_0 = 0.6$ mm.

and forced convection in the burning environment. For SBA and NBA, however, the flames consistently became slightly non-spherical as shown at 0.3 s in Fig. 5, then transitioned to spherical with a blue color as soot formation diminished due to the smaller droplet diameter late in the burning history (cf, 0.5 s in Fig. 5). The origin of this effect is unclear and would benefit from detailed simulations that account for the fiber and soot formation. The trends in the quantitative data discussed in Section 5.2 did not show effects that can convincingly be related to asymmetries in the flame shape.

For burning in the presence of buoyant convection, Fig. 6 shows the flame structure of SBA and NBA droplets (where the actual 'flame' is the luminous portion). There are no obvious differences of flame configuration for the two grades of BA. Both show a hybrid configuration which is due to the buoyant velocity transporting fuel upwards and soot forming in the wake which produces the luminous portion from incandescence when the soot aggregates ignite as they reach the high temperature flame. This leaves the lower hemisphere devoid of soot and the flame has a blue hue there. The sort of stretched flame configuration in Fig. 6 complicates assigning a 'diameter' as a measure of its size, so we do not report flame diameter measurements for the convective droplet case.

The bright lateral streaks in Figs. 5 and 6 are due to the flame intersecting the fiber. The direction in which the flame is viewed makes these streaks visible. The flames appear stretched slightly in the lateral direction in some cases which could be related to an anchoring mechanism for flame holders described in [34]. This stretching effect is only visible in the cross-sectional images in Figs. 5 and 6. The small fiber diameters (14 μm) relative to the droplet size make this flame stretching effect highly localized, and visible only in the imaging direction.

The effect of buoyancy on droplet burning is determined by the relative magnitudes of the velocity induced by fuel evaporation - the 'Stefan' velocity v_s which is in the radial direction - and by density differences between the hot flame and colder ambience, v_b , which is the buoyancy velocity in Fig. 1b. v_b was estimated by a scale analysis by balancing inertia in the momentum equation with buoyancy leading to $v_b \propto \sqrt{g\beta(T_f - T_d)\ell}$ where ℓ is a characteristic length (D_o , D or D_f). For v_s we take the result from the 1-D droplet burning theory where it can be shown that $v_s \propto \frac{\rho_L}{\rho_g} \frac{K_o}{D}$ where K_o is the fuel burning rate. Choosing $\ell = D$,

$$\frac{v_s}{v_b} \propto \frac{\rho_L}{\rho_g} \frac{K_o}{\sqrt{g\beta(T_f - T_d)D^3}} = \frac{1}{Gr^{1/2}} \frac{\rho_L}{\rho_g} \frac{K_o}{\nu} \quad (1)$$

where Gr is the Grashof number, $Gr = \frac{g\beta(T_f - T_d)D^3}{\nu^2}$. As D is reduced the Stefan velocity progressively dominates over the buoyancy induced velocity and the droplet flames should therefore become more spherical. Such a reduction occurs naturally during a given burning event. Fig. 6 shows such a transition late in the burning history. Additionally with a reduction in droplet size, the bright luminous zone in Fig. 6 gradually disappears and the flames become blue which suggests a reduction of soot formation as the droplet becomes smaller by evaporation. The reduced soot formation as a droplet evaporates is consistent with an effect of droplet diameter on the residence time of fuel molecules transported between the droplet and flame [35].

5.2. Quantitative measurements

The evolution of droplet diameter for NBA and SBA is shown in Fig. 7 in scaled coordinates. The derivative of the data gives the fuel burn rate,

$K_{c,o} = \left| \frac{d(D/D_o)^2}{t/D_o^2} \right|$ where the subscripts 'o' and 'c' pertain to burning with minimal convection or strong convection, respectively. The data show

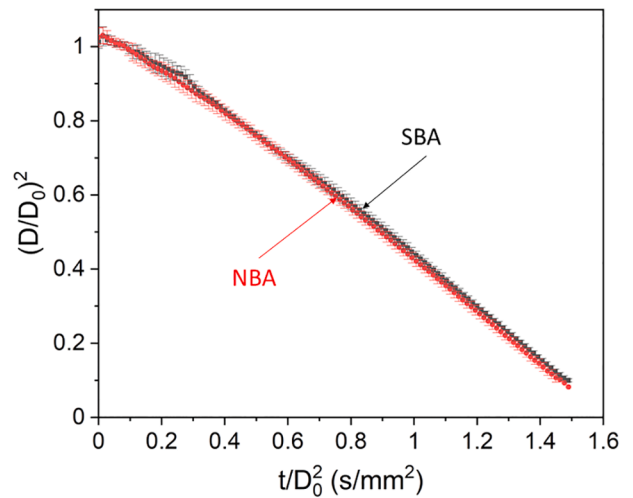


Fig. 7. Comparison of the evolution of averaged scaled droplet diameter with scaled time for NBA and SBA without convection (Fig. 1a).

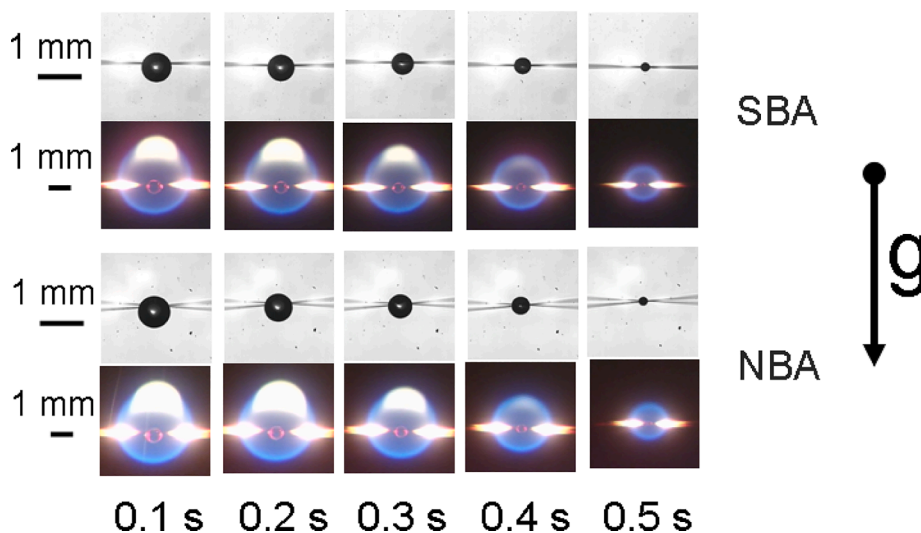


Fig. 6. Time series images of NBA and SBA burning in the presence of buoyant convection. Time after ignition is shown. At 0.4 s the buoyant flames show little evidence of soot and flames are nearly spherical.

that SBA and NBA burning rates are nearly identical and well within experimental uncertainties. The flame diameters (Fig. 8) expressed as the relative distance of the flame to the droplet in Fig. 8, D_f/D_0 , are also virtually identical. These results show that the by-product concentration at 6% (Table 1) is too low to influence burning.

Fig. 9 shows the evolution of droplet diameter of the by-products formed during production of SBA. Differences are significant with hexadecane and *n*-butanol burning the slowest and ethyl acetate the fastest with a burning rate only slightly higher than SBA and NBA. Furthermore, Fig. 10 also shows significant differences in flame positions of the SBA by-products, with by-products having flames closer to the droplet than SBA or NBA flames. These results further show that diluting NBA by 6% has no substantive effect on the physical dynamics of burning in terms of fuel burn rates and relative positions of the droplet flames to the droplet surface.

The evolution of droplet and flame diameters in Figs. 7 and 8 show no evidence of a preferential vaporization effect from the dissolved by-products. However, recent simulations [25] of multicomponent mixtures showed that a preferential vaporization effect can be present even when more global data such as those in Figs. 7 and 8 do not reveal this phenomenon. Without a capability to probe, either by simulation or experiment, the internal composition of SBA droplets, it is not yet evident if preferential vaporization exists during burning of SBA.

In practical applications BA droplets will burn in environments which have significant gas motion created by forced and natural convection. Considering NBA droplets specifically, Fig. 11 compares burning with and without convection. As expected, NBA droplets burn faster with convection. A common correlation for the influence of convection corrects the 1-D fuel burning rate, K_0 , for the effect of convection in the form $K_c = K_0(1 + Gr^n)$ [36], which is consistent with Fig. 11. While K_0 is ostensibly the $Gr = 0$ limit, we do not actually know this limit here because the experiments do not identically achieve $g = 0$ during the free-fall period.

With judicious adjustments of parameters, the convection and convection-free burning configurations (Fig. 1a and 1b) can become coincident. Considering v_B with $\ell = D_0$ as the characteristic length scale, a convective burning effect can be eliminated by reducing D_0 whereby $K_c = K_0$ should result. Taking $D_0 = 0.4$ mm as an example, Fig. 12 shows that the NBA burning rates are now almost identical simply by reducing the droplet diameter.

Fig. 13 compares NBA and SBA burning with convection. The response to convection is essentially the same with no substantive differences. Flame diameter comparisons are not shown because, as noted

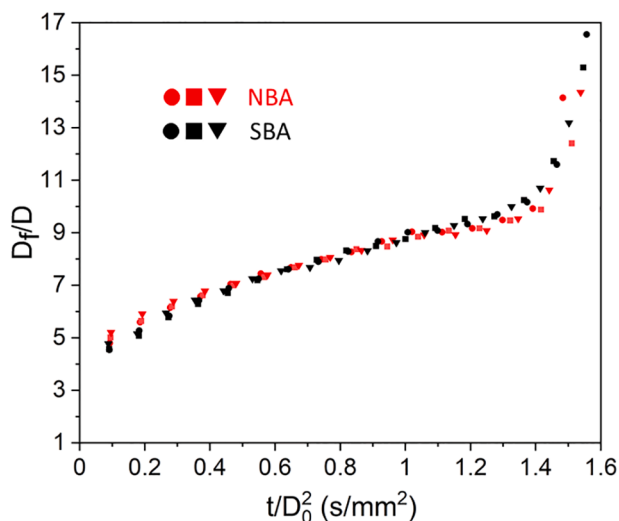


Fig. 8. Comparison of individual NBA and SBA data flame data, D_f/D , without convection (Fig. 1a).

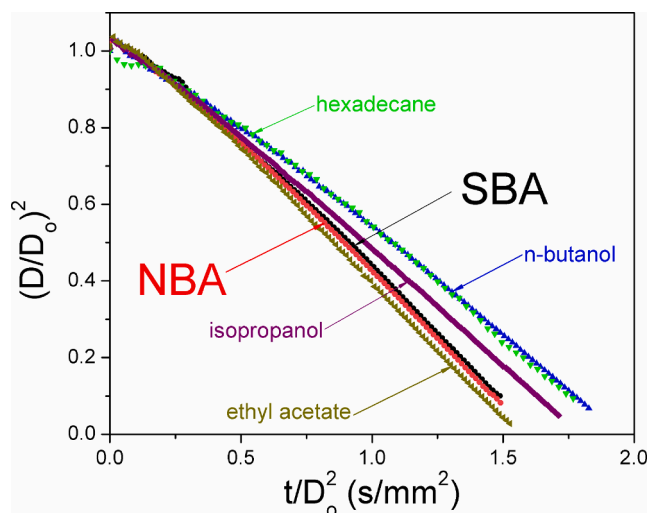


Fig. 9. Evolution of $(D/D_0)^2$ for SBA, NBA and SBA by-products without convection. Data from individual experiments are shown. *n*-butanol data are from [41].

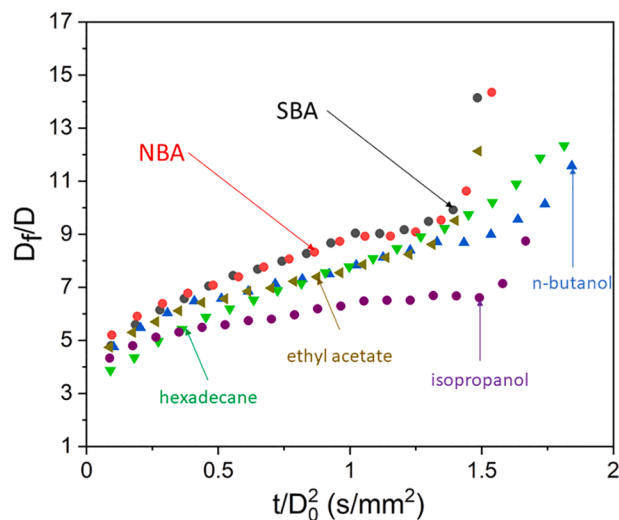


Fig. 10. Evolution of relative position of flame to droplet diameter without convection, D_f/D , for SBA, NBA and SBA by-products. Data from individual experiments are shown. *n*-butanol data from [41].

previously, the buoyant flame shapes would have been ad-hoc constructions.

One aspect of burning where the presence of dissolved species can be a factor, even in small concentrations, is the potential for internal superheating leading to a flash boiling event. We observed that near the end of burning, SBA droplets tended to exhibit a bubbling effect as shown in Fig. 14. Formation of bubbles was not observed for SBA droplets burning without convection (Fig. 11). Nor was it ever observed for NBA droplets with or without convection. The difference appears to be due to the presence of dissolved by-products in SBA with their range of volatilities as listed in Table 1, and the influence of convection on shear-induced internal mixing of components inside the SBA droplets.

A necessary condition to trigger flash boiling is that the temperature of the droplet corresponding to the surface concentration should exceed the boiling point of one or more mixture components inside the droplet [37]. The presence of *n*-hexadecane and its high boiling point makes this viable for SBA. Considering a simplified case in which hexadecane is concentrated at the droplet surface, the SBA droplet temperature could conceivably reach 560 K at atmospheric pressure. This situation can

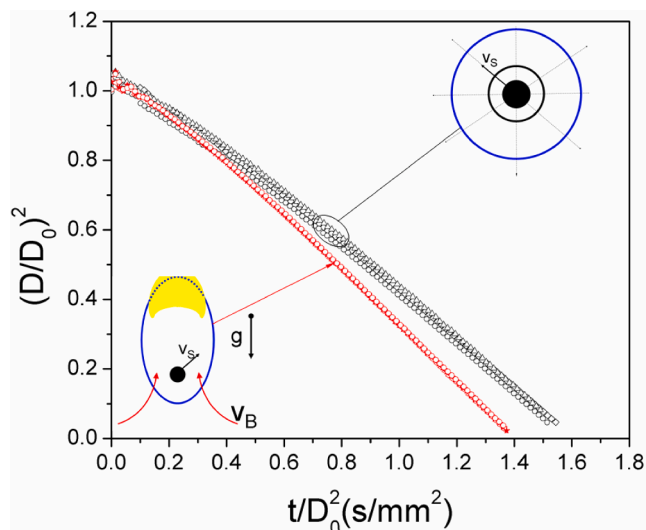


Fig. 11. Comparison of individual runs for NBA burning with and without buoyant convection ($g = 9.8 \text{ m/s}^2$) for $D_o = 0.6 \text{ mm}$. Data from three experiments each are shown.

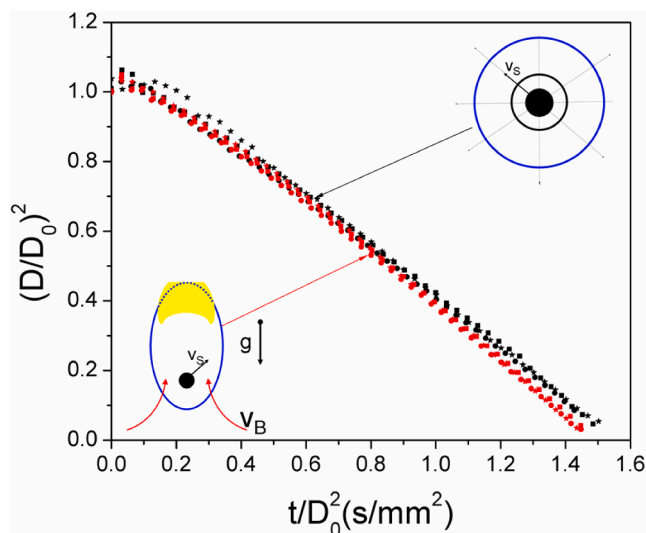


Fig. 12. Comparison of NBA burning with and without buoyant convection for $D_o = 0.4 \text{ mm}$. Data from three experiments each are shown.

arise if the resistance to mass diffusion inside a multicomponent droplet is high enough to trap volatiles inside the droplet [38] or if the shear-induced mixing distributes the dissolved by-products in a way which confines volatile species to the interior of the droplet while the nonvolatile species concentrate at the surface and raise the droplet temperature above the nucleation temperature of the internal volatiles. The fact that NBA never showed flash boiling while it was observed for SBA makes this conjecture viable. Furthermore, there seems to be no possibility for the temperature of a single component liquid to exceed its normal boiling point under an equilibrium vaporization condition.

A simple threshold temperature to trigger bubble nucleation is about 90% of a liquid's critical point [39,40]. Using this criterion, *iso*-propanol, ethyl acetate and *n*-butanol could conceivably become superheated if their transport to the droplet surface is retarded by mass diffusion, or convective mixing keeps these species from the surface. It is

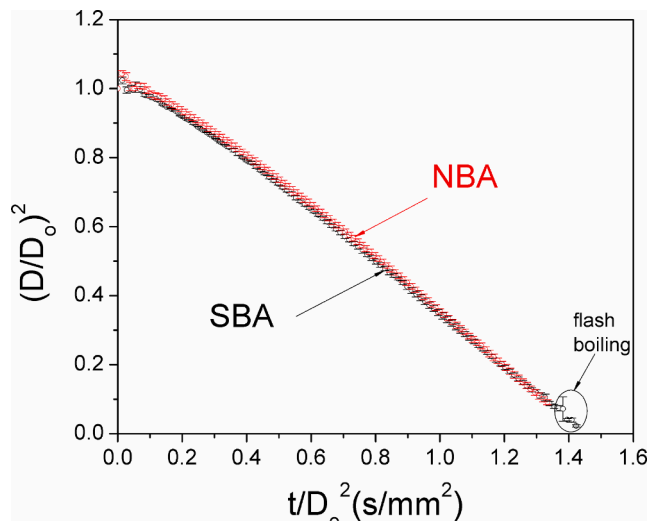


Fig. 13. Comparison of NBA and SBA burning with convection showing flash boiling near the end for SBA.

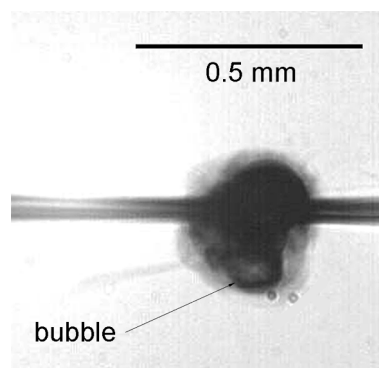


Fig. 14. Photograph of SBA droplet at $t/D_o^2 = 1.41 \text{ s/mm}^2$ after ignition showing internal bubbling. Burning is in the presence of buoyancy-induced convection. NBA droplets did not show this effect.

also noted that the fiber can lower the energetic threshold to trigger flash boiling and the 90% criterion, and this consideration may have also contributed to SBA experiencing internal bubbling.

6. Conclusions

The results presented show that synthesizing butyl acetate by a process that uses a solventogenic *Clostridium* strain through an extractive fermentation process using *n*-hexadecane as the extractant yielded a mixture of butyl acetate and dissolved by-products at just under 6% mass fraction. For burning under conditions that promoted spherical droplet flames through minimizing the influence of external convection, no discernable differences between the burning of SBA and NBA were identified. The droplet burning rates and flame structures were virtually identical between NBA and SBA, though the individual by-product burning processes were different. Similarly, for burning in a convective environment promoted by buoyancy, SBA burning was nearly identical to NBA. No evidence of preferential vaporization was found for SBA, though such an effect is not precluded because concentration gradients inside SBA droplets can still exist. Evidence of disruptive burning was found for SBA which was believed to be due to SBA being

multicomponent and a possible influence of the support fibers. NBA did not show any disruptive burning because it is single component. The study has shown that SBA has burning characteristics almost identical to NBA and is a viable alternative to butyl acetate produced by conventional synthesis processes such as Fischer esterification.

CRedit authorship contribution statement

Yujie Wang: data curation, investigation, validation, formal analysis, visualization, software, writing-original draft, writing-reviewing & editing. **Zhu Chen:** data curation, investigation, validation. **Matthew Haefner:** data curation, investigation, validation, formal analysis, writing original draft, writing-reviewing & editing. **Songtao Guo:** data curation, investigation, visualization, software. **Nicholas DiReda:** data curation, investigation, software. **Yuechao Ma:** data curation, investigation, validation. **Yi Wang:** data curation, investigation, validation, project administration, conceptualization, software, supervision, writing-original draft, writing-reviewing & editing. **C. Thomas Avedisian:** data curation, investigation, validation, formal analysis, conceptualization, methodology, project administration, software, supervision, writing original draft, writing-reviewing & editing.

Declaration of Competing Interest

The authors declare that they have no known competing financial interests or personal relationships that could have appeared to influence the work reported in this paper.

Acknowledgements

The authors acknowledge helpful discussions with Drs. A.J. Agrawal and Josh Bittle of the University of Alabama. The authors also thank the Iowa Central Fuel Testing Laboratory (Fort Dodge, Iowa) for chemical analysis of the bio-synthesized butyl acetate (SBA) used in the present study. This work was supported in part by grants from the Co-Optimization of Fuels & Engines (Co-Optima) program sponsored by the U.S. Department of Energy (DOE), Office of Energy Efficiency and Renewable Energy (EERE), Bioenergy Technologies and Vehicle Technologies Offices (grants DE-EE0008483 and DE-EE0007978) with Dr. Alicia Lindauer as the Program Manager. Additional support was received from the National Aeronautics and Space Administration (grants NNX08AI51G and 80NSSC18K0480) with Dr. Michael C. Hicks as the project monitor.

Appendix A. Supplementary data

Supplementary data to this article can be found online at <https://doi.org/10.1016/j.fuel.2021.121324>.

References

- [1] Boudette NE, Davenport C. G.M. to abandon cars and trucks using gas by 2035. *New York Times*; January 29; 2021. pp. A1, 21.
- [2] Andrade RDA, Faria EA, Silva AM, Araujo WC, Jaime GC, Costa KP, Prado AGS. Heat of combustion of biofuels mixed with fossil diesel oil. *J Therm Anal Calorim* 2011;106:469–74. <https://doi.org/10.1007/s10973-011-1408-x>.
- [3] McCormick RL, Fioroni G, Fouts L, Christensen E, Yanowitz J, Polikarpov E, Albrecht K, Gaspar DJ, Gladden J, George A. Selection criteria and screening of potential biomass-derived streams as fuel blendstocks for advanced spark-ignition engines. *SAE Int J Fuels Lubr* 2017;10:442–60. <https://doi.org/10.4271/2017-01-0868>.
- [4] Gaspar DJ, West BH, Ruddy D, Wilke TJ, Polikarpov E, Alleman TL, George A, Monroe E, Davis RW, Vardon D, Sutton AD, Moore CM, Benavides PT, Dunn J, Bidy MJ, Jones SB, Kass MD, Debusk MM, Sjoberg M, Szybist J, Sluder CS, Fioroni G, Pitz WJ. Top ten blendstocks derived from biomass for turbocharged spark ignition engines: bio-blendstocks with potential for highest engine efficiency, Report No. PNNL-28713, Pacific Northwest National Laboratory; 2019. (see also <https://www.osti.gov/servlets/purl/1567705>).
- [5] Miles P. Efficiency Merit Function for Spark Ignition Engines: Revisions and 1094 Improvements Based on FY16–17 Research, Report No. DOE/GO-102018-5041, 1095 U.S. Department of Energy; 2018. (see also <https://www.nrel.gov/docs/fy18osti/67584.pdf>).
- [6] Rodriguez GM, Tashiro Y, Atsumi S. Expanding ester biosynthesis in *Escherichia coli*. *Nat Chem Biol* 2014;10:259–65. <https://doi.org/10.1038/nchembio.1476>.
- [7] van den Berg C, Heeres AS, van der Wielen LAM, Straathof AJJ. Simultaneous clostridial fermentation, lipase-catalyzed esterification, and ester extraction to enrich diesel with butyl butyrate. *Biotechnol Bioeng* 2013;110:137–42. <https://doi.org/10.1002/bit.24618>.
- [8] Westbrook CK, Pitz WJ, Curran HJ. Chemical kinetic modeling study of the effects of oxygenated hydrocarbons on soot emissions from diesel engines. *J Phys Chem A* 2006;110:6912–22. <https://doi.org/10.1021/jp056362g>.
- [9] U.S. Energy Information Administration. Diesel fuel explained, see <https://www.eia.gov/energyexplained/diesel-fuel/>, June 12; 2020.
- [10] Ali SH, Al-Rashed O, Azeez FA, Merchant SQ. Potential biofuel additive from renewable sources – Kinetic study of formation of butyl acetate by heterogeneously catalyzed transesterification of ethyl acetate with butanol. *Bioresour Tech* 2011; 102:10094–103. <https://doi.org/10.1016/j.biortech.2011.08.033>.
- [11] Liu Y, Lotero E, Goodwin JG. Effect of water on sulfuric acid catalyzed esterification. *J Mol Catal A: Chem* 2006;245:132–40. <https://doi.org/10.1016/j.molcata.2005.09.049>.
- [12] Li WB, Wang JX, Gong H. Catalytic combustion of VOCs on non-noble metal catalysts. *Catal Today* 2009;148:81–7. <https://doi.org/10.1016/j.cattod.2009.03.007>.
- [13] Linz H-G, Wittstock K. Catalytic combustion of solvent-containing air on base metal catalysts. *Catal Today* 1996;27:237–42. [https://doi.org/10.1016/0920-5861\(95\)00193-X](https://doi.org/10.1016/0920-5861(95)00193-X).
- [14] Lintz H-G, Wittstock K. The oxidation of solvents in air on oxidic catalysts — formation of intermediates and reaction network. *Applied Catal A: General* 2001; 216:217–25. [https://doi.org/10.1016/S0926-860X\(01\)00572-5](https://doi.org/10.1016/S0926-860X(01)00572-5).
- [15] Musialik-Piotrowska A, Syczewska K. Combustion of volatile organic compounds in two-component mixtures over monolithic perovskite catalysts. *Catal Today* 2000; 59:269–78. [https://doi.org/10.1016/S0920-5861\(00\)00293-5](https://doi.org/10.1016/S0920-5861(00)00293-5).
- [16] Parus W, Paterkowski W. Catalytic oxidation of organic pollutants. *Polish J Chem Tech* 2009;11:30–7. <https://doi.org/10.2478/v10026-009-0040-z>.
- [17] Takamitsu Y, Yoshida S, Kobayashi W, Ogawa H, Sano T. Combustion of volatile organic compounds over composite catalyst of Pt/ γ -Al₂O₃ and beta zeolite. *J Environ Sci Health A* 2013;48:667–74. <https://doi.org/10.1080/10934529.2013.744563>.
- [18] Tan X, Lan H, Xie H, Zhou G, Jiang Y. Role of surface oxygen species of mesoporous CeCu oxide catalyst in OVOCs catalytic combustion. *J Environ Chem Eng* 2017;5: 2068–76. <https://doi.org/10.1016/j.jece.2017.03.033>.
- [19] Wong CT, Abdullah AZ, Bhatia S. Catalytic oxidation of butyl acetate over silver-loaded zeolites. *J Hazardous Mater* 2008;157:480–9. <https://doi.org/10.1016/j.jhazmat.2008.01.012>.
- [20] Imai T, Anderson RB. Decomposition of *n*- and *sec*-butyl acetates on synthetic zeolites II. Kinetics and Mechanism. *Product R&D* 1973;12:232–7. <https://doi.org/10.1021/i360047a014>.
- [21] Pettit PJ, Anderson RB. Decomposition of *n*- and *iso*-butyl acetates on charcoal. *Can J Chem Eng* 1978;56:218–22. <https://doi.org/10.1002/cjce.5450560209>.
- [22] Feng J, Zhang J, Ma Y, Feng Y, Wang S, Guo N, Wang H, Wang P, Jiménez-Bonilla P, Gu Y, Zhou J, Zhang ZT, Cao M, Jiang D, Wang S, Liu X, Shao Z, Borovik I, Huang H, Wang Y. Renewable fatty acid ester production in *Clostridium*. *Nature Commun* 2021. <https://doi.org/10.1038/s41467-021-24038-3>.
- [23] Reid RC, Prausnitz JM, Poling BE. *The properties of gases and liquids*. 4th ed. New York: McGraw-Hill; 1987.
- [24] Haylett DR, Lappas PP, Davidson DF, Hanson RK. Application of an aerosol shock tube to the measurement of diesel ignition delay times. *Proc Combust Inst* 2009;32: 477–84. <https://doi.org/10.1016/j.proci.2008.06.134>.
- [25] Cuoci A, Avedisian CT, Brunson JD, Guo S, Dalili A, Wang Y, Mehl M, Frassoldati A, Seshadri K, Dec JE, Lopez-Pintor D. Simulating combustion of a seven-component surrogate for a gasoline/ethanol blend including soot formation and comparison with experiments. *Fuel* 2021;288:119451. <https://doi.org/10.1016/j.fuel.2020.119451>.
- [26] Dalili A, Brunson JD, Guo S, Turello M, Pizetti F, Badiali L, Avedisian CT, Seshadri K, Cuoci A, Williams FA, Frassoldati A, Hicks MC. The role of composition in the combustion of *n*-heptane/*iso*-butanol mixtures: experiments and detailed modelling. *Combust Theory Model* 2020;24(6):1002–20. <https://doi.org/10.1080/13647830.2020.1800823>.
- [27] Liu YC, Alam FE, Xu Y, Dryer FL, Avedisian CT, Farouk TI. Combustion characteristics of butanol isomers in multiphase droplet configurations. *Combust Flame* 2016;169:216–28. <https://doi.org/10.1016/j.combustflame.2016.04.018>.
- [28] Farouk TI, Liu YC, Savas AJ, Avedisian CT, Dryer FL. Sub-millimeter sized methyl butanoate droplet combustion: Microgravity experiments and detailed numerical modeling. *Proc Combust Inst* 2013;34:1609–16. <https://doi.org/10.1016/j.proci.2012.07.074>.
- [29] Liu YC, Avedisian CT. A comparison of the spherical flame characteristics of sub-millimeter droplets of binary mixtures of *n*-heptane/*iso*-octane and *n*-heptane/toluene with a commercial unleaded gasoline. *Combust Flame* 2012;159:770–83. <https://doi.org/10.1016/j.combustflame.2011.08.015>.
- [30] Liu YC, Xu Y, Hicks MC, Avedisian CT. Comprehensive study of initial diameter effects and other observations on convection-free droplet combustion in the standard atmosphere for *n*-heptane, *n*-octane, and *n*-decane. *Combust Flame* 2016; 171:27–41. <https://doi.org/10.1016/j.combustflame.2016.05.013>.

- [31] Dembia CL, Liu YC, Avedisian CT. Automated data analysis of consecutive digital images from droplet combustion experiments by a MATLAB-based algorithm. *Image Anal Stereol* 2012;31:137. <https://doi.org/10.5566/ias.v31.p137-148>.
- [32] Mueller CJ, Martin GC. Effects of Oxygenated Compounds on Combustion and Soot Evolution in a DI Diesel Engine: Broadband Natural Luminosity Imaging, 2002, p. 2002-01-1631. <https://doi.org/10.4271/2002-01-1631>.
- [33] Glassman I. *Combustion*. 3rd ed. San Diego: Academic Press; 1996. p. 270.
- [34] Wan J, Zhao H, Akkerman V. Anchoring mechanisms of a holder-stabilized premixed flame in a preheated mesoscale combustor. *Phys Fluids* 2020;32:097103. <https://doi.org/10.1063/5.0021864>.
- [35] Jackson GS, Avedisian CT, Yang JC. Observations of soot during droplet combustion at low gravity: heptane and heptane/monochloroalkane mixtures. *Int J Heat Mass Tran* 1992;35:2017-33. [https://doi.org/10.1016/0017-9310\(92\)90203-5](https://doi.org/10.1016/0017-9310(92)90203-5).
- [36] Sadhal SS, Ayyaswamy PS, Chung JN. *Transport phenomena with drops and bubbles*. New York: Springer-Verlag; 1997. p. 102.
- [37] Avedisian CT, Skyllingstad K, Cavicchi RC, Lippe C, Carrier MJ. Initiation of flash boiling of multicomponent miscible mixtures with application to transportation fuels and their surrogates. *Energy&Fuels* 2018;32:9971-81. <https://doi.org/10.1021/acs.energyfuels.8b02258>.
- [38] Makino A, Law CK. On the controlling parameter in the gasification behavior of multicomponent droplets. *Combust Flame* 1988;73:331-6. [https://doi.org/10.1016/0010-2180\(88\)90027-2](https://doi.org/10.1016/0010-2180(88)90027-2).
- [39] Avedisian CT. The homogeneous nucleation limits of liquids. *J of Phys Chem Ref Data* 1985;14:695-729. <https://doi.org/10.1063/1.555734>.
- [40] Skripov VP. *Metestable liquids*. New York: John Wiley & Sons; 1974.
- [41] Xu Y, Avedisian CT. Combustion of n-butanol, gasoline, and n-butanol/gasoline mixture droplets. *Energy Fuels* 2015;29:3467-75. <https://doi.org/10.1021/acs.energyfuels.5b00158>.